Penning Ionization of Cyclic Ethers by Collision with He*(2^3S) Metastable Atoms

Masayo Yamauchi, Hideo Yamakado, and Koichi Ohno*

Department of Chemistry, Graduate School of Science, Tohoku University, Aramaki, Aoba-ku, Sendai 980-77, Japan

Received: December 4, 1996; In Final Form: April 1, 1997[⊗]

Penning ionization of tetrahydropyran, tetrahydrofuran, 1,4-dioxane, and 1,3-dioxane upon collision with He*-(2^3S) atoms was studied by collision-energy-resolved Penning ionization electron spectroscopy. In the studied energy range, the interaction potential around the oxygen atoms was found to be attractive and anisotropic depending on the in-plane and the out-of-plane access of He*, in good agreement with model potential calculations. Observed collision energy dependence of partial Penning ionization cross sections can be related to the molecular orbital of which ionization occurs and also to local interaction potentials where the electron distribution of the molecular orbital is mainly exposed to the outside. Effects of attractive interaction potentials around the oxygen atoms were found to depend on the stereochemical surroundings. Enhancement of PIES intensity was commonly found for C_{2s} bands and some π_{CO} bands of studied cyclic ethers. On the basis of these findings, assignments of ultraviolet photoelectron spectra were discussed.

I. Introduction

Penning ionization[1] is a kind of chemionization in which a molecule M collides with a metastable atom A* having an excitation energy much larger than the lowest ionization potential (IP) of the molecule. This ionization process yields the ground state atom A, an ionic state of the molecule M_i^+, and an ejected electron e^-:

$$A^* + M \rightarrow A + M_i^+ + e^- \quad (1)$$

Since Penning ionization is a collisional ionization process,[2,3] it reflects the interaction potential between a metastable atom and a target molecule. One of the methods to obtain the information about the interaction potential is the measurement of the collision energy dependence of Penning ionization cross sections. There have been various studies in previous years[4−11] for atoms and simple molecules collided with metastable atoms. The positive collision energy dependence of ionization cross sections has been obtained for the collision of Ar atom with He*,[4−8] indicating the interaction potential is repulsive. On the other hand, the negative collision energy dependence is observed for Hg atom with He* [2,4,8] where the interaction potential is attractive.

If a target system is an atom, the interaction potential is isotropic, but in the case of a target molecule, there is an anisotropy of the interaction potential. In this case, it is difficult to obtain information on anisotropy from the study of total ionization cross section, and techniques for specification of the reaction sites are desirable.

In Penning ionization electron spectroscopy (PIES),[12] the kinetic energies of electrons ejected by Penning ionization are analyzed. Because of the electron transfer ionization mechanism of Penning ionization process,[13] PIES provides the information on the electron distribution of individual molecular orbitals exposed outside the molecular surface (van der Waals surface).[14] Since the molecular orbitals are (more or less) localized on a special part of the target molecule, the final ionic state-selected collision energy dependence reflects the anisotropic characteristics of the interaction potential.

Recently, novel techniques including detection of state-resolved Penning electrons as a function of velocity of metastable atoms[15−21] have been developed. Using time-of-flight (TOF) selections of metastable atoms, we have obtained collision energy dependence of partial ionization cross sections σ (E_C), and we have reported information on the anisotropy of the interaction potential.[15−18]

By means of these techniques, we found a very anisotropic potential surface for He*(2^3S) with various organic compounds.[22−27] These investigations suggest consistently that the interaction potential strongly depends on geometrical surroundings of atoms or chemical groups. In our previous study of CH_3OH, $(CH_3)_2O$, and $(CH_3CH_2)_2O$ upon collision with He*-(2^3S),[26] we found that the potential surface around the lone-pair electrons localized on the oxygen atoms is attractive and the surface around the methyl group is repulsive. It was also found that the attractive interaction around the oxy group becomes weaker as the substituents become larger; in $(CH_3CH_2)_2O$, attractive interaction was observed to be weaker in comparison with CH_3OH or $(CH_3)_2O$. This may be attributed to the difference of steric hindrance around the oxygen atom. In order to confirm the effect of geometrical surroundings of the reaction sites, we selected in this study four cyclic ethers, tetrahydropyran ($C_5H_{10}O$), tetrahydrofuran (C_4H_8O), 1,4-dioxane ($C_4H_8O_2$), and 1,3-dioxane ($C_4H_8O_2$), with relatively similar chemical composition to $(CH_3CH_2)_2O$ but having less rotational freedom of CH_2-groups and bare oxy groups. Along with this purpose, the spectral assignments and PIES characteristics of these cyclic ethers were also studied.

II. Experimental Section

The experimental apparatus used in this study has been reported previously in detail.[15−18] The metastable atoms of He*-(2^3S, 2^1S) were produced by a discharge nozzle source, and the He*(2^1S) component was eliminated by a water-cooled helium discharge lamp. The kinetic energy distribution of ejected electrons was analyzed by a hemispherical electrostatic deflection type analyzer[28] using an electron collection angle to the incident beam axis of 90°. The resolution of the electron energy analyzer was estimated to be 40 meV from the full widths at half-maximum (fwhm) of the $Ar^+(^2P_{3/2})$ peak in the

[⊗] Abstract published in *Advance ACS Abstracts,* August 1, 1997.

S1089-5639(96)03980-1 CCC: $14.00

He I ultraviolet photoelectron spectrum (UPS). The transmission efficiency curve of the electron energy analyzer was determined by comparing our UPS data with those of Gardner and Samson[29] and Kimura et al.[30]

In collision-energy-resolved measurements, the He*(2^3S) metastable beam was pulsed with a mechanical chopper and introduced to the collision cell. The time-of-flight signal (TOF) of He*(2^3S) I_M was obtained by detecting secondary electrons emitted from stainless steel plate inserted into the collision cell. TOFs of secondary electrons from metal surface to the detector are negligibly short in comparison with TOFs of He*(2^3S) atoms.

In order to obtain a collision-energy-resolved PIES (CERPIES), two spectra with a low collision energy of about 95 meV and with a high collision energy of about 230 meV were measured by selecting Penning electrons with certain range of TOF. The resolution of the analyzer was lowered to 250 meV (fwhm for He I UPS of Ar) to obtain higher counting rates.

The time-dependent spectrum of Penning electrons for a given ionic state I_E was measured using the energy fixed mode of the electron analyzer (fwhm for He I UPS of Ar was 250 meV) in order to determine the collision energy dependence of the partial ionization cross sections (CEDPICS). Since the time-resolved spectrum gives the electron intensity I_E as a function of the velocity v_M of He*(2^3S), the partial ionization cross section $\sigma(E_C)$ can be determined by the equations:

$$\sigma(v_R) = c\{I_E(v_M)/I_M(v_M)\}\,(v_M/v_R) \tag{2}$$

$$v_R = \{v_M{}^2 + 3\,k_B\,T/m\}^{1/2} \tag{3}$$

where c is a constant, v_R is the relative velocity averaged over the velocity of the target molecule, k_B is the Boltzmann constant, and T and m are the gas temperature and the mass of the target molecule, respectively. Finally, $\sigma(v_R)$ is converted to $\sigma(E_C)$ by the relation

$$E_C = \mu v_R{}^2/2 \tag{4}$$

where μ is the reduced mass of the system.

III. Calculations

In order to discuss the band assignment and relative band intensity observed in PIES, ab initio molecular orbital (MO) calculations were performed with 4-31G basis functions utilizing a program package.[31] The geometries of neutral target molecules used for calculations were selected from the literature.[32−35]

Interaction potential curves with metastable atom approaching the oxygen atom along several directions were calculated for discussion about observed collision energy dependence by using ab initio MO method in the scheme of the unrestricted Hartree−Fock (UHF). A 4-31++G** basis set was used.

Although calculations involving an excited atom of He*(2^3S) are usually very difficult because of the highly excited complex system, there are well-known resemblance between He*(2^3S) atom and Li(2^2S) atom. It has been shown[36] that the shape of velocity dependence of the total scattering cross sections of He*(2^3S) by He, Ar, and Kr is very similar to shape those of Li(2^2S). The interaction potential well depths and the location of potential well have also been found to be similar for interactions of various target with He*(2^3S) and Li(2^2S) (see refs 2, 16, 37, and 38 and references cited therein). In this study we used a Li atom instead of He* atom for the model calculation of interaction potentials in order to avoid the difficulties associated with calculations for excited states.

IV. Simple Model for Collision Energy Dependence of Partial Ionization Cross Sections

If the simple theoretical models[2] established for isotropic target systems can also be applied effectively to anisotropic systems, collision energy dependence of partial ionization cross sections (CEDPICS) for molecular systems can be related to interaction potentials and electronic transition probability as described below.

The negative slope m of the log σ vs log E_c plot is related to the attractive potential well. When the long-range attractive part of the interaction potential $V^*(R)$ plays a dominant role, and its function form is the type of

$$V^*(R) \propto R^{-s} \tag{5}$$

$\sigma(E_C)$ can be represented[2,4,9] by

$$\sigma(E_C) \propto E_C{}^{-2/s} \tag{6}$$

In this case, the slope m of the log σ vs log E_C plot is negative.

If the repulsive part of the interaction potential governs the energy dependence, $\sigma(E_C)$ can be derived[4] as

$$\sigma(E_C) \propto (\ln E_C/C)^2 (E_C/C)^{b/d-1/2} \tag{7}$$

on the basis of the assumption of simple analytical forms for the interaction potential $V^*(R)$ and electronic transition probability $w(R)$,

$$w(R) = A\exp(-bR) \tag{8}$$

$$V^*(R) = C\exp(-dR) \tag{9}$$

When the minor energy dependence of the first factor in eq 7 is neglected, the positive slope m of the log σ vs log E_C plots can be related roughly to the two parameter, b and d in eqs 8 and 9.

$$m = b/d - {}^1/_2 \tag{10}$$

The parameter b can be estimated from asympotic decay of the target wave function,[16] which is directly related to the lowest ionization potential (IP) of the molecule.[39,40]

$$b = 2(2\mathrm{IP})^{1/2} \tag{11}$$

The positive slope parameter m is therefore related to the parameter d. The parameter d represents the effective steepness of the repulsive potential wall.

V. Results

Figures 1−4 show the He I ultraviolet photoelectron spectra (UPS) and Penning ionization electron spectra (PIES) of tetrahydropyran, tetrahydrofuran, 1,4-dioxane, and 1,3-dioxane, respectively. The electron energy scales for PIES are shifted relative to those for the UPS by the difference in the excitation energies, 21.22 − 19.82 = 1.40 eV. The present He I UPS and He*(2^3S) PIES are consistent with the earlier data.[30,41−46]

Figures 5−8 show collision-energy-resolved Penning ionization electron spectra (CERPIES) of tetrahydrofuran, tetrahydrofuran, 1,4-dioxane, and 1,3-dioxane, respectively. In each figure, the low collision energy spectrum (ca. 95 meV) is shown by a solid curve and the high collision energy spectrum (ca. 230 meV) is shown by a dashed curve. The relative intensities of the two spectra are normalized in the figures using the data of the log σ vs log E_C plots.

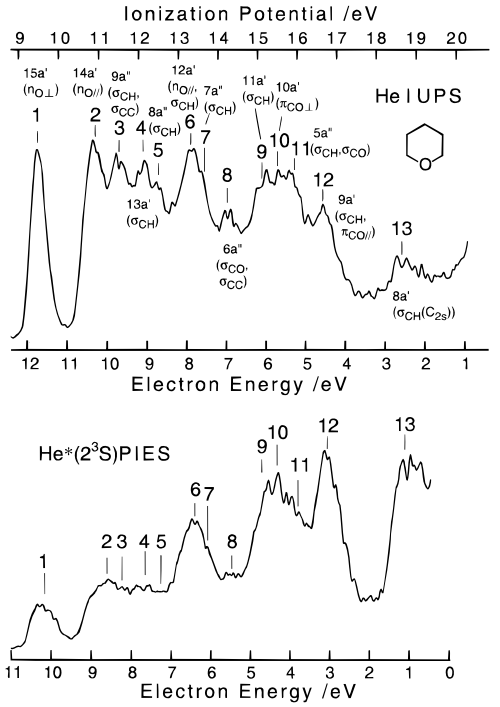

Figure 1. He I UPS and He*(2^3S) PIES of tetrahydropyran.

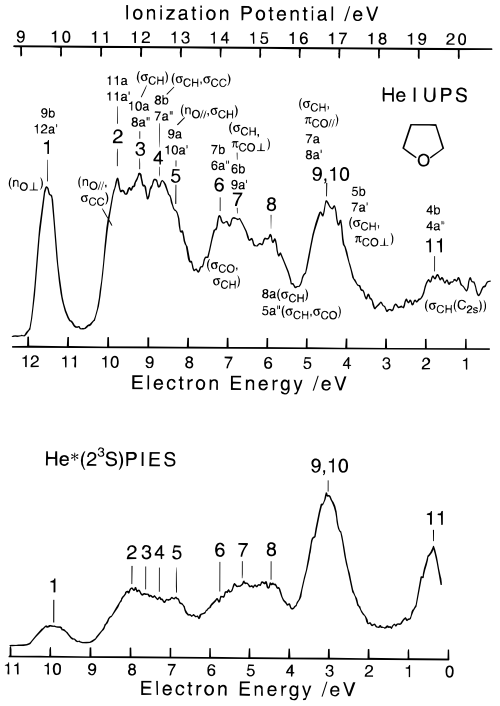

Figure 2. He I UPS and He*(2^3S) PIES of tetrahydrofuran.

Tables 1−4 list the vertical ionization potentials (determined from He I UPS) and the assignments of observed bands. The peak energy shifts in PIES measured with respect to the nominal energy E_0 (E_0 = the difference between metastable excitation energy and target ionization potential) are also shown in Tables 1−4. The peak energy shifts reflect the interaction potential between He* and the target molecule.[47] When the interaction potential is attractive, the ejected electron kinetic energy is smaller than E_0 and the negative peak energy shift in PIES is obtained. When the interaction potential is repulsive, the positive peak energy shift is obtained.

Figures 9−12 show the log σ vs log E_C plots for tetrahydropyran, tetrahydrofuran, 1,4-dioxane, and 1,3-dioxane, respectively. The calculated electron density contour maps and schematic representations of the molecular orbitals are also

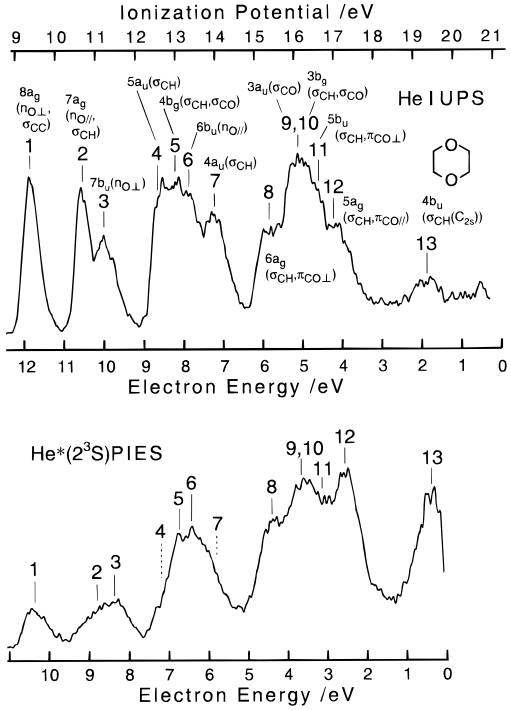

Figure 3. He I UPS and He*(2^3S) PIES of 1,4-dioxane.

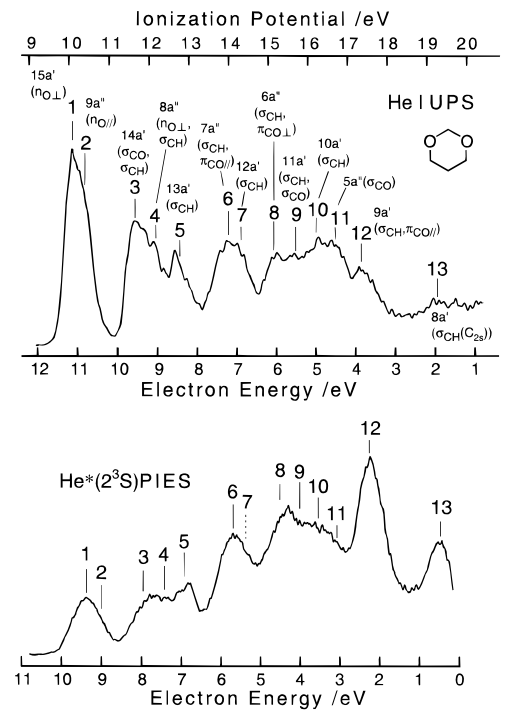

Figure 4. He I UPS and He*(2^3S) PIES of 1,3-dioxane.

shown in the figures. The thick solid lines in the electron density map represent the molecular surface estimated from van der Waals radii of component atoms. In the contour map several cutting planes are used according to the orbital character. The values of the slope m of the log σ vs log E_C plots are also listed in Tables 1−4. The slope parameter m was estimated in a collision energy range of 70−400 meV. The error for the value of m was estimated to be ±0.03.

Figures 13−15 show interaction potential energy curves $V^*(R)$ obtained from the model potential calculations of Li + tetrahydropyran and Li + tetrahydrofuran when the Li atom access the oxygen atom from (a) in-plane direction of COC plane and (b) out-of-plane direction of COC plane. R is the distance between the Li atom and O atom.

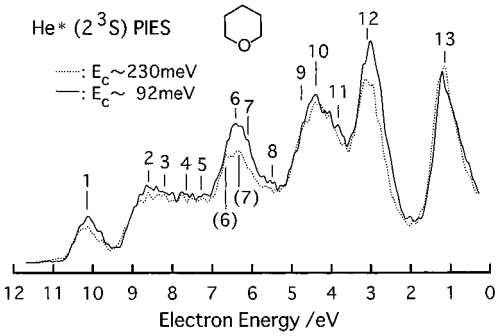

Figure 5. Collision-energy-resolved He*(2^3S) Penning ionization electron spectra of tetrahydrofuran [(—) 71−113 meV, average 92 meV; (···) 177−403 meV, average 230 meV]. For bands 6 and 7, two peaks are clearly observed in high collision energy spectrum, although they are not clearly resolved in UPS.

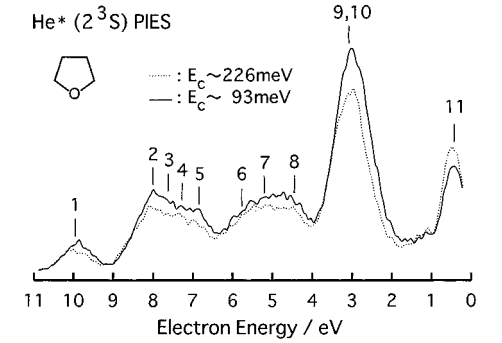

Figure 6. Collision-energy-resolved He*(2^3S) Penning ionization electron spectra of tetrahydrofuran [(—) 71−114 meV, average 93 meV; (···) 174−395 meV, average 226 meV].

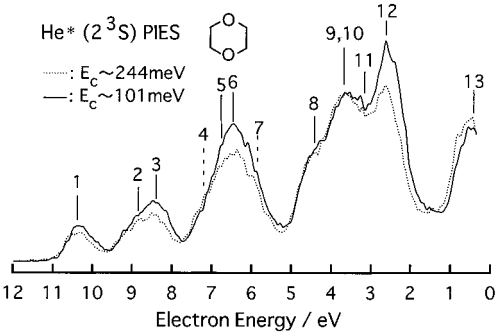

Figure 7. Collision-energy-resolved He*(2^3S) Penning ionization electron spectra of 1,4-dioxane [(—) 74−127 meV, average 101 meV; (···) 188−464 meV, average 244 meV].

VI. Discussion

A. Tetrahydropyran. The UPS of tetrahydropyran have been extensively investigated,[30,41,42] but assignments have been proposed for only three bands.[41] Table 1 lists the present assignments based upon the CEDPICS and the CERPIES. In our assignments, 13 bands are contained in the energy range of He I UPS, though previously Kimura et al.[30] have suggested 10 bands. As clearly seen in Figure 1, bands 4 and 5 are contained in the range of 12−13 eV in IP. Bands 6 and 7 are contained in the range of 13−14 eV in IP, since two peaks are clearly seen in the high collision energy spectrum in CERPIES (Figure 5), though they are not resolved in UPS. For the broad peak in 15−16 eV in IP, we assigned three bands. Although the assignments for bands 6 and 7 are different from those resulting from the sequence of calculated orbital energies, the reason is described below.

The largest negative slope of collision energy dependence in Figure 9 is observed in band 1 ($m = -0.258$). The band 1 originates from ionization of 15a′ ($n_{O\perp}$) orbital. The orbital

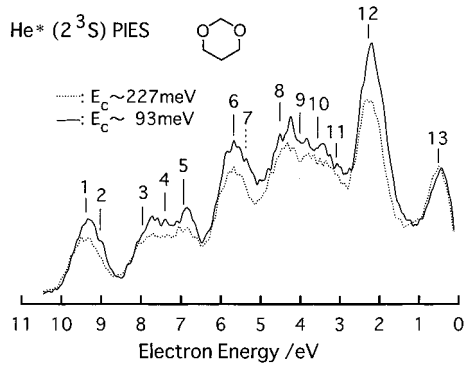

Figure 8. Collision-energy-resolved He*(2^3S) Penning ionization electron spectra of 1,3-dioxane [(—) 71−113 meV, average 93 meV) (···) 174−390 meV, average 227 meV].

TABLE 1: Band Assignments, Ionization Potentials, Peak Energy Shifts, and Obtained Parameter Values for Tetrahydropyran[a]

band	obsd, IP/eV	calcd, IP/eV	orbital	character	peak energy shift/meV	*m*
1	9.46	10.85	15a′	$n_{O\perp}$	−200 ± 50	−0.258
2	10.93	11.81	14a′	$n_{O\parallel}$	−300 ± 150	−0.125
3	11.52	12.18	9a″	σ_{CH}(eq),σ_{CC}	−80 ± 150	
4	12.10	13.09	13a′	σ_{CH}(ax)	−80 ± 150	−0.026
5	12.50	13.42	8a″	σ_{CH}(ax)	−70 ± 150	
6	13.32	14.65	12a′	$n_{O\parallel}$,σ_{CH}(eq)	−110 ± 150	−0.226
7	13.63	14.54	7a″	σ_{CH}(eq)	−100 ± 150	
8	14.25	15.76	6a″	σ_{CO},σ_{CC}	−120 ± 150	−0.037
9	15.06	16.61	11a′	σ_{CH}(ax,eq)	0 ± 150	
10	15.52	17.13	10a′	$\pi_{CO\perp}$	0 ± 150	−0.016
11	15.90	17.18	5a″	σ_{CH}(ax),σ_{CO}	−100 ± 150	
12	16.66	18.27	9a′	σ_{CH}(eq)$\pi_{CO\parallel}$	−120 ± 100	−0.218
13	18.63	20.87	8a′	σ_{CH}(ax)(C_{2s})	−100 ± 150	0.060

[a] See text.

character is oxygen lone pair extending around the oxygen atom in perpendicular directions from the COC plane. Since the electron density is distributed outside the molecular surface selectively around the oxygen atom, the slope $|m|$ is the largest in this compound reflecting attractive interaction around the oxygen atom. This attractive interaction is also confirmed from negative peak energy shift (−200 ± 50 meV) observed in PIES.

The bands 2, 3 ($m = 0.125$), 6, 7 ($m = -0.226$), and 12 ($m = -0.218$) are assigned to 14a′($n_{O\parallel}$), 9a″(σ_{CH}(eq),σ_{CC}), 12a′($n_{O\parallel}$,σ_{CH}(eq)), 7a″(σ_{CH}(eq)), and 9a′(σ_{CH}(eq),$\pi_{CO\parallel}$) (eq = equatorial) orbitals, respectively. The set of these bands show the next largest inclination of CEDPICS. This is quite reasonable because bands 2, 6, and 12 correspond to the orbitals extending outside along with the COC plane around the oxygen atom. A little flatter slopes compared with band 1 are attributed to the repulsive interaction around the hydrogen atoms, because bands 3, 7, and 12 correspond to σ_{CH} orbitals have electron distributions extending around equatorial hydrogen atoms.

The bands 2 and 3 are overlapping in PIES, though clearly resolved in UPS, because of a large negative peak shift of −300 ± 150 meV for the band 2 originating from attractive interaction in comparison with a smaller shift for the band 3. The negative peak shift of band 2 is larger than that of band 1. As discussed in section E, this is because the exterior electron density of 14a′($n_{O\parallel}$) orbital is distributed in the deep attractive potential well region and also because the He* atom is more directly affected by the attractive interaction potential compared with the case of 15a′($n_{O\perp}$) orbital. The slope *m* for the bands 2 and 3 is smaller than band 1 because of the contribution of the band 3 originated from σ_{CH}(eq),σ_{CC} orbital.

The intensity of bands 6 and 7 is relatively large in PIES because of the exterior electron distribution extending out-

TABLE 2: Band Assignments, Ionization Potentials, Peak Energy Shifts, and Obtained Parameter Values for Tetrahydrofuran[a]

band	obsd, IP/eV	C_2 calcd, IP/eV	orbital	character	C_s calcd, IP/eV	orbital	character	peak energy shift/meV	*m*
1	9.67	10.97	9b	$n_{O\perp}$	11.26	12a′	$n_{O\perp}$	-230 ± 50	−0.460
2	11.41	12.33	11a	$n_{O\parallel},\sigma_{CC}$	12.45	11a′	$n_{O\parallel},\sigma_{CC}$	-430 ± 150	−0.200
3	11.99	12.97	10a	σ_{CH}	12.69	8a″	σ_{CH}	-210 ± 150	
4	12.48	13.21	8b	σ_{CH},σ_{CC}	13.17	7a″	σ_{CH},σ_{CC}	-70 ± 150	−0.222
5	12.90	13.48	9a	$n_{O\parallel},\sigma_{CH}$	13.43	10a′	$n_{O\parallel},\sigma_{CH}$	-70 ± 150	
6	14.00	15.21	7b	σ_{CO},σ_{CH}	14.93	6a″	σ_{CO},σ_{CH}	-70 ± 150	−0.154
7	14.45	16.09	6b	$\sigma_{CH},\pi_{CO\perp}$	15.92	9a′	$\sigma_{CH},\pi_{CO\perp}$	-190 ± 200	
8	15.29	16.18	8a	σ_{CH}	16.62	5a″	σ_{CH},σ_{CO}	-60 ± 150	−0.093
9	16.70	18.06	7a	$\sigma_{CH},\pi_{CO\parallel}$	18.05	8a′	$\sigma_{CH},\pi_{CO\parallel}$	-80 ± 100	−0.220
10	16.70	18.71	5b	$\sigma_{CH},\pi_{CO\perp}$	18.65	7a′	$\sigma_{CH},\pi_{CO\perp}$	-80 ± 100	
11	19.42	21.85	4b	$\sigma_{CH}(C_{2s})$	21.60	4a″	$\sigma_{CH}(C_{2s})$	0 ± 100	0.184

[a] See text.

TABLE 3: Band Assignments, Ionization Potentials, Peak Energy Shifts, and Obtained Parameter Values for 1,4-Dioxane[a]

band	obsd, IP/eV	calcd, IP/eV	orbital	character	peak energy shift/meV	*m*
1	9.37	10.56	$8a_g$	$n_{O\perp},\sigma_{CC}$	-80 ± 50	−0.235
2	10.67	12.08	$7a_g$	$n_{O\parallel},\sigma_{CH}$(ax,eq)	-350 ± 150	−0.117
3	11.20	12.36	$7b_u$	$n_{O\perp}$	-250 ± 150	−0.277
4	12.57	14.03	$5a_u$	σ_{CH}(ax)		−0.133
5	12.99	14.06	$4b_g$	σ_{CH}(eq),σ_{CO}	-80 ± 150	
6	13.34	14.64	$6b_u$	$n_{O\parallel}$	-60 ± 150	−0.300
7	14.05	15.21	$4a_u$	σ_{CH}(eq)		−0.228
8	15.37	17.28	$6a_g$	σ_{CH}(ax),$\pi_{CO\perp}$	-50 ± 150	−0.101
9	16.1	17.35	$3a_u$	σ_{CO}	-60 ± 150	
10	16.1	17.73	$3b_g$	σ_{CH}(ax),σ_{CO}	-60 ± 150	−0.023
11	16.62	17.80	$5b_u$	σ_{CH}(eq),$\pi_{CO\perp}$	-80 ± 150	
12	17.00	18.96	$5a_g$	σ_{CH}(eq),$\pi_{CO\parallel}$	-260 ± 100	−0.293
13	19.33	21.76	$4b_u$	σ_{CH}(ax)(C_{2s})	-110 ± 150	0.037

[a] See text.

TABLE 4: Band Assignments, Ionization Potentials, Peak Energy Shifts, and Obtained Parameter Values for 1,3-Dioxane[a]

band	obsd, IP/eV	calcd, IP/eV	orbital	character	peak energy shift/meV	*m*
1	10.08	11.44	15a′	$n_{O\perp}$	-370 ± 150	−0.315
2	10.39	11.56	9a″	$n_{O\parallel}$	-410 ± 150	
3	11.66	12.74	14a′	σ_{CO},σ_{CH}(eq)	-210 ± 150	−0.262
4	12.18	12.95	8a″	$n_{O\perp},\sigma_{CH}$(ax)	-240 ± 150	
5	12.79	13.85	13a′	σ_{CH}(ax)	-120 ± 150	−0.313
6	14.00	15.37	7a″	σ_{CH}(eq),$\pi_{CO\parallel}$	-130 ± 150	−0.258
7	14.31	15.66	12a′	σ_{CH}(eq)		
8	15.15	16.94	6a″	σ_{CH}(ax,eq),$\pi_{CO\perp}$	-150 ± 150	−0.165
9	15.72	17.16	11a′	σ_{CH}(eq),σ_{CO}	-100 ± 150	
10	16.19	17.88	10a′	σ_{CH}(ax)	-100 ± 150	−0.124
11	16.68	18.10	5a″	σ_{CO}	-70 ± 150	
12	17.35	19.21	9a′	σ_{CH}(eq),$\pi_{CO\parallel}$	-200 ± 100	−0.237
13	19.30	21.75	8a′	σ_{CH}(ax)(C_{2s})	-80 ± 150	0.015

[a] See text.

side around the oxygen atom (12a′) and of the distribution around the equatorial hydrogen atoms of α and β carbon in common phase (7a″). The stronger band 6 is assigned to the 12a′($n_{O\parallel},\sigma_{CH}$(eq)) orbital which has larger exterior electron distribution than that of 7a″(σ_{CH}(eq)) orbital.

Since the corresponding 9a′(σ_{CH}(eq),$\pi_{CO\parallel}$) orbital has a large electron distribution extending widely along the COC plane without nodes (Figure 9), the intensity of band 12 in PIES is very large. For this band, the collision occurs both around equatorial hydrogen atoms and with this the in-plane direction around the oxygen atom. The negative collision energy dependence is similar to that of bands 2, 3 and 6, 7 which also reflect the interaction both around the oxygen and the hydrogen atoms.

The slope of CEDPICS for bands 4 and 5 is almost flat ($m = -0.026$) which indicates that the repulsive interaction is dominant. This is consistent with the σ_{CH}(ax) (ax = axial) character of corresponding 13a′ and 8a″ orbitals and also with very small peak energy shifts for these bands. Since the PIES intensity for bands 4 and 5 is smaller than the bands 2 and 3, the reactivity around the axial hydrogen atoms is considered to be smaller than the equatorial hydrogen atoms.

The band 8 is relatively weak in PIES. This band is assigned to 6a″(σ_{CO},σ_{CC}) orbital which makes the molecular ring skeleton.

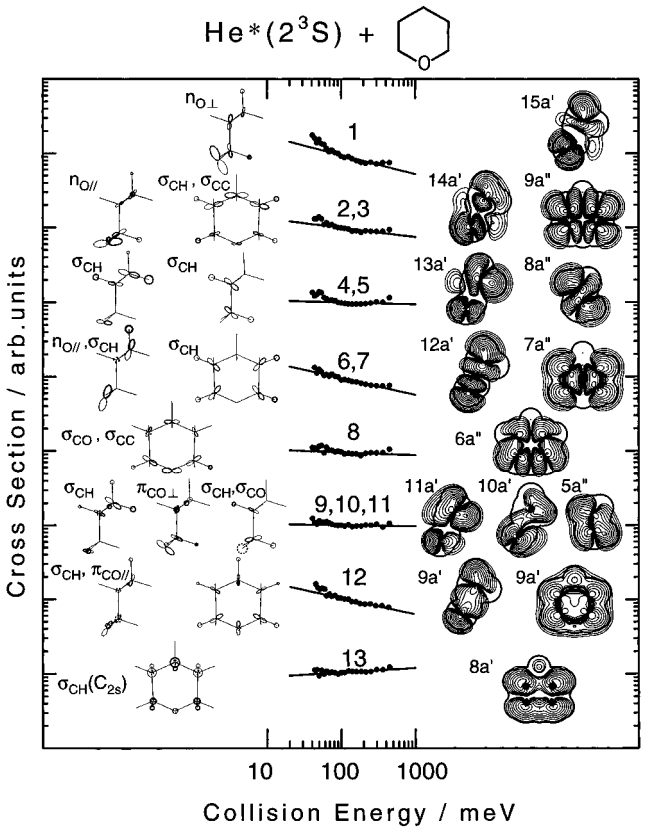

Figure 9. Collision-energy dependence of partial ionization cross sections for tetrahydropyran with He*(2^3S). The experimental collision energy dependence (log σ vs log E_C plots) for corresponding PIES bands are plotted in dots. The slope *m* is determined in the range of 70−400 meV. To the left of the log σ vs log E_C plots the schematic representations of molecular orbitals corresponding to the PIES bands are shown. To the right the electron density contour maps for respective MO are shown. The thick solid lines in contour maps represent the molecular surface. The cutting planes of contour maps are the C_s symmetric plane for 15a′, 14a′, 13a′, 12a′, 11a′, 10a′, and 9a′ orbitals, and the plane including four carbon atoms for 9a″, 7a″, 6a″, 9a′, and 8a′ orbitals. The plane including CC bond axis and perpendicular to the plane of four carbon atoms are selected for 8a″ and 5a″ orbitals. The direction of the molecule in the schematic representation and the contour map are the same for each orbital. For 9a′ orbital, two schematic representations and contour maps correspond to different directions are shown.

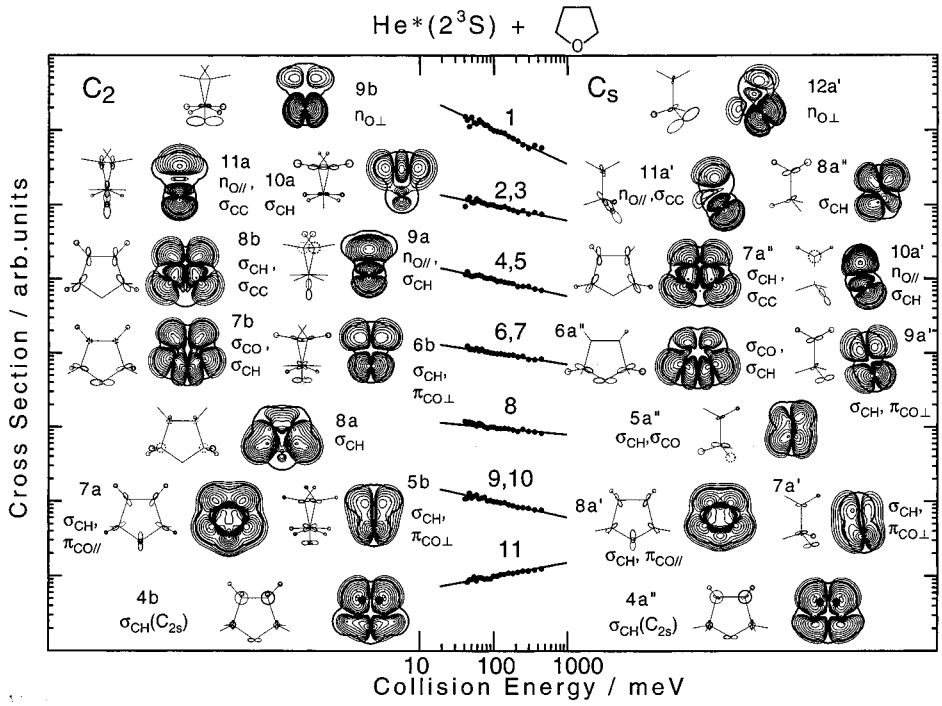

Figure 10. Collision-energy dependence of partial ionization cross sections for tetrahydrofuran with He*(2^3S). To the left of the log σ vs log E_C plots the schematic representations and contour maps for C_2 conformer are shown. To the right, those for C_s conformer are shown. The cutting plane of contour maps are as follows: (a) the plane bisecting the COC plane for 9b, 11a, 10a, 9a, 6b, 5b, 12a′, 11a′, 10a′, 9a′, and 7a′ orbitals, (b) the plane including COC plane for 8b, 7b, and 7a orbitals, (c) the plane including oxygen atom and β-carbon atoms for 8a and 4b orbitals, (e) the plane including four carbon atoms for 7a″, 6a″, 8a′, and 4a″ orbitals, (f) the plane containing CC bond axis for 8a″ and 5a″ orbitals.

Because the electron density is distributed mainly in the bonding region, the intensity of this band is very small. Collision energy dependence is almost flat because the reaction occurs at the equatorial hydrogen atoms although the reactivity is low.

The bands 9, 10, and 11 are assigned to 11a′(σ_{CH}(ax,eq), 10a′-($\pi_{CO\perp}$), 5a″(σ_{CH}(ax),σ_{CO}), respectively. The average slope m of the log σ vs log E_C plot for these bands is almost flat ($m = -0.016$) because of the relatively large contribution of σ_{CH} character in these orbitals as in the case of bands 4 and 5. The band 9, which shows little difference between low and high collision energy spectra (Figure 5), is assigned to 11a′(σ_{CH}(ax,eq)) orbital. Since negative collision energy dependence for the band 10 is larger than for band 9, the band 10 should be assigned to 10a′($\pi_{CO\perp}$) orbital, which has relatively high electron density area around the oxygen atom. Relatively small PIES band intensity for the band 11 suggests the corresponding orbital has relatively small electron density outside the molecular surface. Thus the band 11 is assigned to 5a″(σ_{CH}(ax),σ_{CO}) orbital.

The band 13 is very weak in UPS but very enhanced in PIES (Figure 1). This band is assigned to the 8a′(σ_{CH}(ax)(C_{2s})) orbital. The slope of the log σ vs log E_C plot of band 13 is positive in good contrast to other bands, because the reaction site is localized on carbon atoms and also because interaction potential is repulsive and soft. The enhancement in PIES is explained by the C_{2s} character in this orbital, which concentrates electron density on the inner valence of four carbon atoms. Takami et al. observed this enhancement in PIES of σ_{CH}(C_{2s}) orbital of neopentane and explained that the excitation transfer between He* and the target followed by intramolecular Auger-like ionization process would occur.[48] Because the overlap of two intramolecular orbitals which participate this ionization process is much larger than intermolecular orbital overlap which leads to usual Penning ionization, the band intensity becomes much larger. In the case of cyclic ethers the enhancement of C_{2s} band in PIES is the key of the assignment of the overall spectral range of the He I UPS.

B. Tetrahydrofuran. Although the UPS[30,43,44] and the PIES[46] of tetrahydrofuran have been measured, no assignment has been proposed except for the first band. Our assignments are listed in Table 2. Kimura et al.[30] have suggested 9 bands in the spectral range of He I UPS, but there are 11 bands in our assignments. We assigned at 12.90 eV in IP as band 5 in the UPS, which is seen as a shoulder in the UPS but clearly observed in PIES. From the MO calculation, the bands 9 and 10 are assigned to the peak at 16.70 eV in IP, and the band 11 is assigned to the peak at 19.42 eV.

The structure of tetrahydrofuran in the gas phase have long been investigated, both theoretically[49−52] and experimentally.[33,53,54] In the recent study using ab initio calculations,[51] C_2 structure (half-chair, or twisted conformation) is in the energy minimum and C_s structure (envelop conformation) is only 0.3 kcal/mol higher. According to this, the gaseous sample is the mixture containing 63% of C_2 conformer and 37% of C_s conformer at room temperature. As shown in Table 2, the orbital energies and MO characters of these two conformers resemble each other. The calculated interaction potential with He* access to the oxygen atom (Figures 14 and 15) are also similar to each other. Thus the following discussions are based on the major conformer of the C_2 type.

The tendency of the slope of CEDPICS for tetrahydrofuran shown in Figure 10 can be explained as in the case of tetrahydropyran as discussed below. The negative slope of band 1, corresponding to $n_{O\perp}$ orbital (9b for C_2 conformer) is the largest ($m = -0.460$). The 9b orbital has its electron distribution mainly around the oxygen atom. As in the case of tetrahydropyran, the large negative slope indicates that the interaction potential around the oxygen atom is attractive. The large negative peak shift of -230 ± 50 meV and band broadening in PIES in Figure 2 are also consistent with the attractive interaction potential. The large negative slope of band 1 in tetrahydrofuran compared with tetrahydropyran is related to the difference in conformations and the difference in interaction potentials, as described in section E.

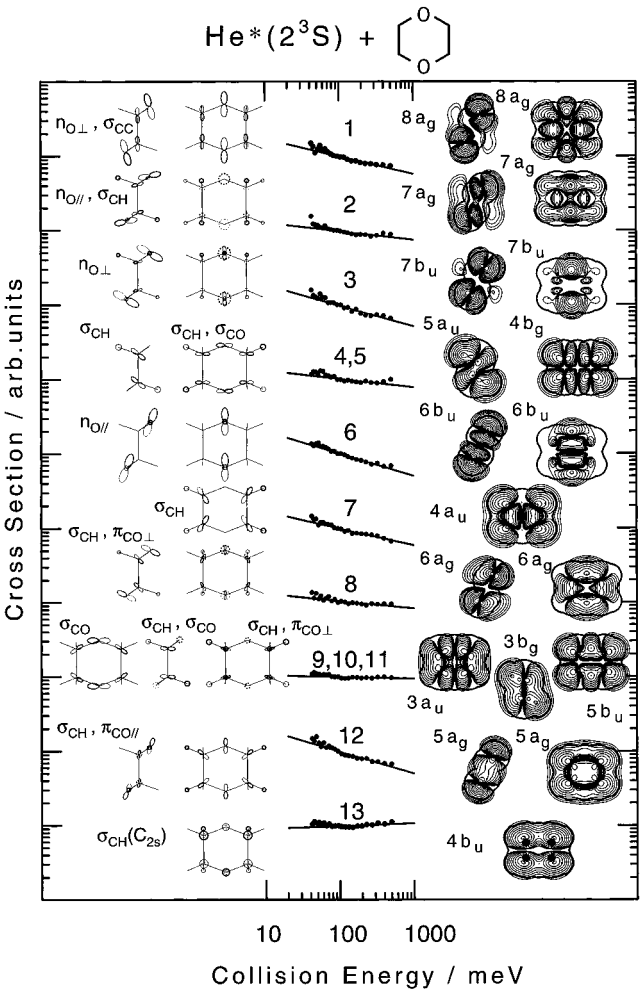

Figure 11. Collision-energy dependence of partial ionization cross sections for 1,4-dioxane collided with He*(2^3S). The cutting planes of contour maps are as follows: the plane including four carbon atoms is selected for $8a_g$, $7a_g$, $7b_u$, $4b_g$, $6b_u$, $4a_u$, $6a_g$, $3a_u$, $5b_u$, $5a_g$, and $4b_u$ orbitals, the C_s symmetric plane is for $8a_g$, $7a_g$, $7b_u$, $6b_u$, $6a_g$, and $5a_g$ orbitals, the plane including CC bond axis and perpendicular to the plane of four carbon atoms is for $5a_u$ and $3b_g$ orbitals. Two schematic representations and contour maps corresponding to different directions are shown for $8a_g$, $7a_g$, $7b_u$, $6b_u$, $6a_g$, and $5a_g$ orbitals.

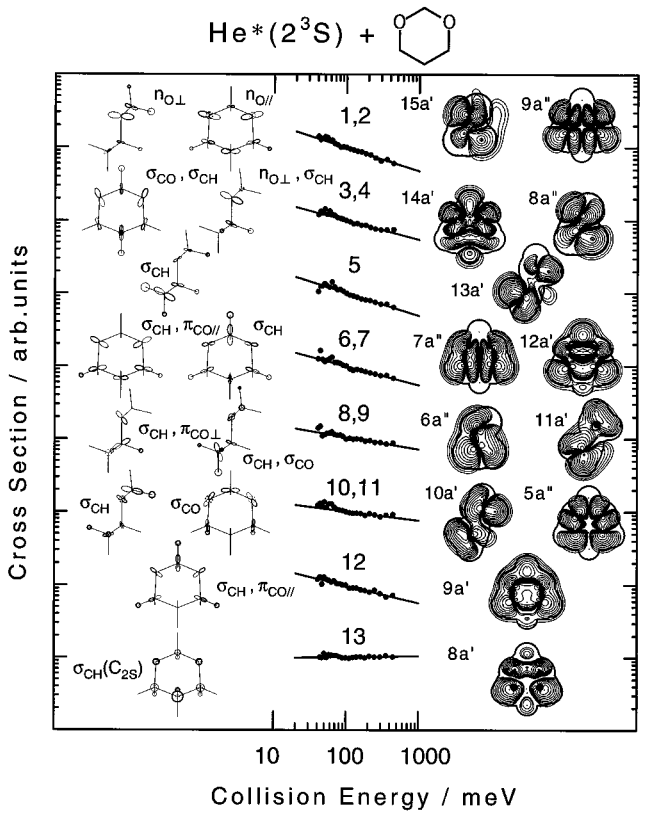

Figure 12. Collision-energy dependence of partial ionization cross sections for 1,3-dioxane collided with He*(2^3S). The cutting planes of contour maps are the C_s symmetric plane for 13a′, 11a′, and 10a′ orbitals and the plane including two oxygen and two carbon atoms for 9a″, 14a′, 7a″, 12a′, 5a″, 9a′, and 8a′ orbitals. The plane including CO bond axis and perpendicular to the plane of two oxygen and two carbon atoms are selected for 15a′, 8a″, and 6a″ orbitals.

The next largest negative slopes of CEDPICS are obtained for the bands 2, 3 ($m = -0.200$), 4, 5 ($m = -0.222$), and 9, 10 ($m = -0.220$). As for the bands 2, 3 and 4, 5, two types of bands due to $n_{O||}$ (band 2, band 5) and σ_{CH} (band 3, band 4) orbitals are overlapping. The bands 9 and 10 correspond to σ_{CH},$\pi_{CO||}$ and σ_{CH},$\pi_{CO\perp}$ orbitals. The negative slope of CEDPICS for these bands is relatively large reflecting attractive interaction around the oxygen atom but smaller than band 1, because repulsive interaction around the hydrogen atoms is involved.

The bands 2 and 3 are resolved in UPS but overlapped in PIES (Figure 2). The band 2 is assigned to the 11a($n_{O||}$,σ_{CC}) orbital, extending along the COC plane around the oxygen atom. The very large negative peak energy shift of band 2 in PIES is consistent with the strong attractive interaction within the COC plane around the oxygen atoms, as in the case of tetrahydropyran. The band 3 having smaller peak energy shift is assigned to the 10a(σ_{CH}) orbital which is mainly distributed around the hydrogen of β-carbon atoms. As can be seen in the CERPIES (Figure 6), the negative collision energy dependence is larger in band 2 than band 3, which is also consistent with this assignment.

For slope m of bands 4 and 5, an explanation similar to the case of bands 2 and 3 can be made. The band 5 originates from orbital 9a($n_{O||}$,σ_{CH}), and band 4 originates from the 8b orbital (σ_{CH},σ_{CC}). The band 5 should be assigned to the orbital having larger exterior electron distribution around the oxygen atom, because the band 5 shows slightly larger negative collision energy dependence than the band 4 (Figure 6).

The bands 9 and 10 are assigned to 7a(σ_{CH},$\pi_{CO||}$) and 5b-(σ_{CH},$\pi_{CO\perp}$) orbitals. The 7a(σ_{CH},$\pi_{CO||}$) orbital is extending to a parallel direction along the COC plane in the same phase, which resembles 9a′ orbital of tetrahydropyran. The 5b(σ_{CH},$\pi_{CO\perp}$) orbital is extending outside the COC plane. The high intensity in PIES indicates that the exterior electron distribution of these orbitals is large. The PIES enhancement of π_{CO} orbitals have also observed in the case of $(CH_3)_2O$ and $(CH_3CH_2)_2O$.[26]

As for the bands 6 and 7, the negative slope of CEDPICS is relatively small ($m = -0.154$), because it reflects relatively large electron distribution around the hydrogen atoms in the corresponding orbitals. The band 6 is assigned to 7b(σ_{CO},σ_{CH}) orbital, which localizes the electron density in the bonding region and around the hydrogen atoms of α-carbon. The PIES intensity is small because the electron distribution extends outside around the oxygen atom is very small. On the other hand, 6b(σ_{CH},$\pi_{CO\perp}$) orbital extends outside, both around the hydrogen and oxygen atoms. Thus the band 7 should be assigned to the 6b(σ_{CH},$\pi_{CO\perp}$) orbital, since it shows larger negative peak energy shift and relatively larger collision energy dependence than band 6 (Figure 6) reflecting attractive interaction. The PIES intensity is relatively higher than band 6 (Figure 2).

The band 8 is originated from 8a(σ_{CH}) orbital. The ionization reaction occurs mainly around the hydrogen atoms and the attractive effect on the interaction potential around oxygen is very small. Thus the collision energy dependence is small ($m = -0.093$).

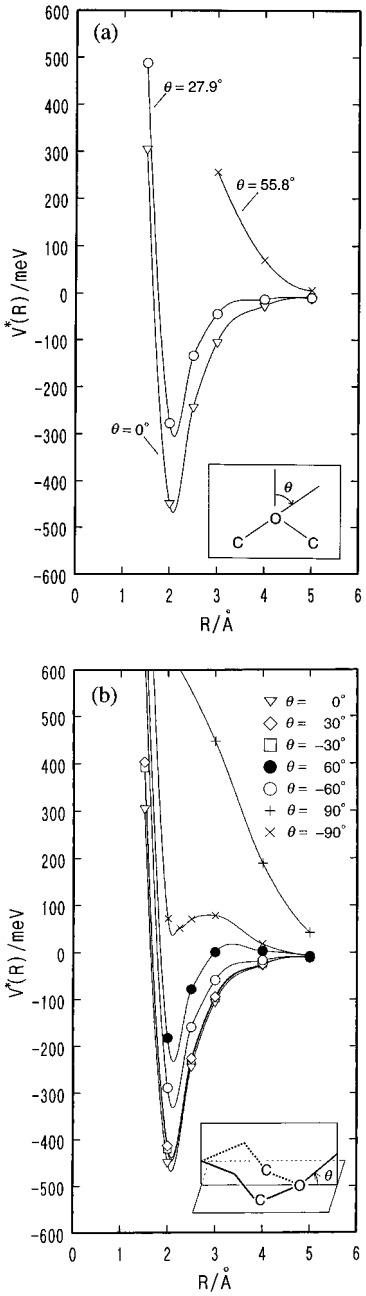

Figure 13. Model potential curves $V^*(R)$ for tetrahydropyran with Li in the level of UHF: (a) the potential energy curve for the in-plane access to an oxygen atom, (b) the potential energy curve for the out-of-plane access to an oxygen atom.

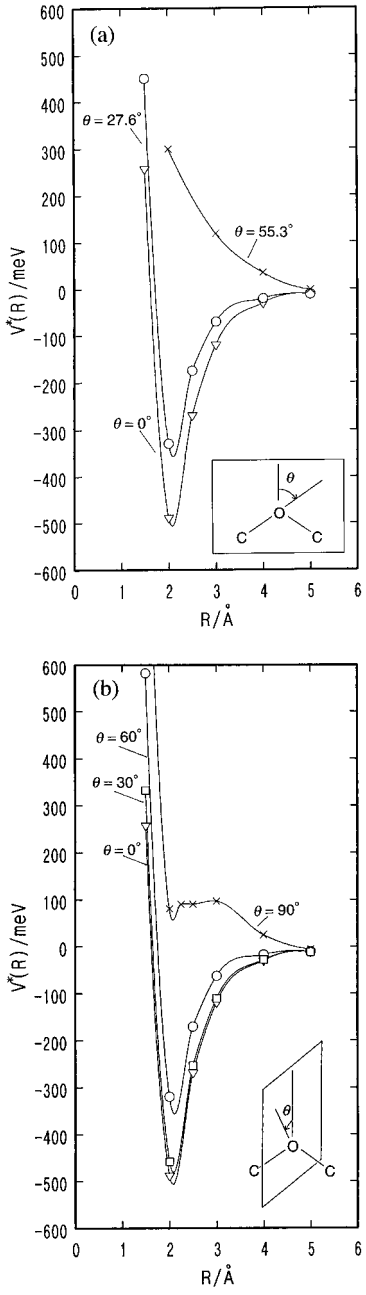

Figure 14. Model potential curves $V^*(R)$ for tetrahydrofuran (C_2) with Li in the level of UHF: (a) the potential energy curve for the in-plane access to an oxygen atom, (b) the potential energy curve for the out-of-plane access to an oxygen atom.

The band 11 shows an enhancement in PIES. This band should be assigned to $\sigma_{CH}(C_{2s})$ orbital having large electron distribution mainly on the β-carbon atoms, because the slope of CEDPICS is also positive as observed in the corresponding band in tetrahydropyran (band 13 in Figure 9).

C. 1,4-Dioxane. The He I[30,41,42] UPS and He* PIES[46] of 1,4-dioxane is previously investigated, but assignments of only a few bands have been suggested. On the basis of the UPS including He II and a semiempirical calculation, assignments of He II UPS bands have been proposed.[45] Our assignments of UPS are summarized in Table 3.

The collision energy dependence of partial ionization cross sections for 1,4-dioxane can be related to the attractive interaction around the oxygen atoms, as in the case of tetrahydropyran. The largest negative slopes of CEDPICS in Figure 11 are observed for the bands 3, ($m = -0.277$), 6 ($m = -0.300$), and 12 ($m = -0.293$). Since the corresponding MO characters of bands 3 and 6 are $n_{O\perp}$ and $n_{O\parallel}$, the interaction potential around the oxygen atoms is considered to be attractive both out-of plane and in-plane directions of the COC planes. The band 12 corresponds to an orbital extending around the oxygen atoms in the COC planes where the interaction potential is highly attractive.

The band 1 is assigned to $8a_g(n_{O\perp},\sigma_{CC})$ orbital. Negative peak energy shift in PIES and negative slope of m corresponding to attractive interaction around the oxygen atoms are observed. The relatively small value of $|m|$ with respect to band $3(n_{O\perp})$, as well as small peak energy shift of -80 ± 50 meV, can be related to a certain amount of the exterior electron density of $8a_g(n_{O\perp},\sigma_{CC})$ orbital around the axial and equatorial hydrogen atoms (Figure 11), where the interaction potential is rather repulsive.

The band 2 is assigned to $7a_g(n_{O\parallel},\sigma_{CH}(ax,eq))$ orbital, although it has been assigned to b_u orbital in the semiempirical calculation.[45] Negative slope of m and the large negative peak shift of -350 ± 150 meV corresponds to attractive interaction

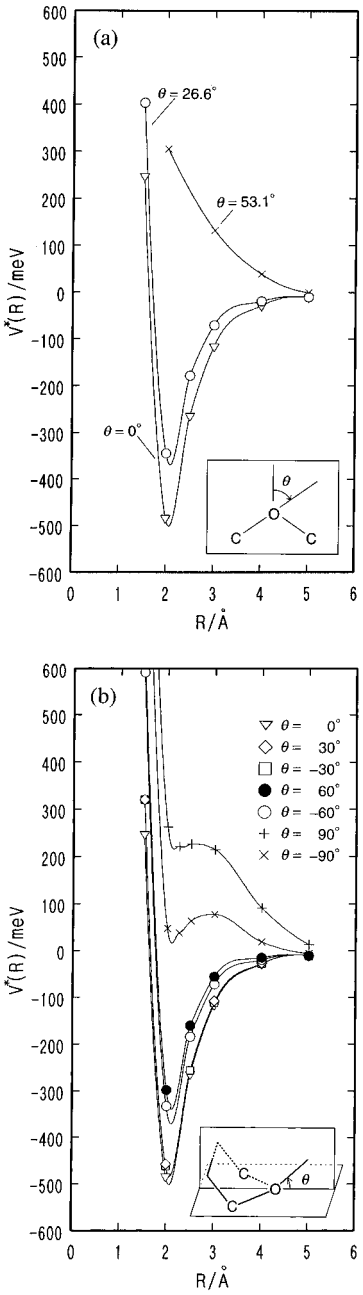

Figure 15. Model potential curves $V^*(R)$ for tetrahydrofuran (C_s) with Li in the level of UHF: (a) the potential energy curve for the in-plane access to an oxygen atom, (b) the potential energy curve for the out-of-plane access to an oxygen atom.

around the oxygen atoms in COC plane were obtained as in the case of the band 6 ($6b_u$,$n_{O\parallel}$). The slope of m ($m = -0.117$) is smaller compared with that of the band 6 because the electron distribution around the axial and equatorial hydrogen atoms are larger for the $7a_g$($n_{O\parallel}$,σ_{CH}(ax,eq)) orbital. Furthermore, the electron distribution of $7a_g$($n_{O\parallel}$,σ_{CH}(ax,eq)) orbital much less extends outside around the oxygen atoms than the $6b_u$($n_{O\parallel}$) orbital.

The band 3 is originated from $7b_u$($n_{O\perp}$) orbital. The exterior electron distribution of this orbital is mostly around the oxygen atoms. The large negative slope of m and negative peak energy shift directly reflect attractive interaction around the oxygen atoms.

The bands 4 and 5 are originated from axial and equatorial σ_{CH} orbitals, respectively. The negative slope of collision energy dependence is small, reflecting the contribution of repulsive interaction around the hydrogen atoms. The band 5 is assigned to the $4b_g$(σ_{CH}(eq),σ_{CO}) orbital and has larger PIES intensity and larger collision energy dependence compared with the band 4.

The band 6 is originated from $6b_u$($n_{O\parallel}$) orbital. This orbital has large electron distribution in the COC planes around the oxygen atoms. The negative slope of CEDPICS for this band ($m = -0.300$) is the largest in this molecule even though there are band-overlapping, and this is considered to reflect the local interaction around the oxygen atoms. This indicates that the effect of attractive potential is stronger in the parallel direction rather than perpendicular direction of COC planes. The strong band intensity in PIES is due to the large exterior electron distribution of the corresponding orbital.

The band 7 is originated from $4a_u$(σ_{CH}(eq)) orbital, which extends along the direction of equatorial hydrogen atoms. The band 7 is clearly resolved in UPS but overlapping in PIES because of the weaker PIES intensity than that of band 6. The CEDPICS of the band 7 shows relatively large negative slope due to the overlapping of the neighboring strong band 6.

The band 8 corresponds to $6a_g$(σ_{CH}(ax),$\pi_{CO\perp}$) orbital. Although electron density of $6a_g$(σ_{CH}(ax),$\pi_{CO\perp}$) orbital is distributed around the oxygen atoms as that of $7b_u$($n_{O\perp}$) orbital, the exterior electron distribution around the axial hydrogen atoms is considered to be larger than that of 7 bu orbital. Thus the CEDPICS for the band 8 shows much smaller negative slope than that in the case of band 3.

The bands 9, 10, and 11 correspond to $3a_u$(σ_{CO}), $3b_g$-(σ_{CH}(ax),σ_{CO}) and $5b_u$(σ_{CH}(eq),$\pi_{CO\perp}$) orbitals, respectively. The $3a_u$(σ_{CO}) orbital has relatively small exterior electron distribution due to the bonding character of the ring skeleton. The $3b_g$-(σ_{CH}(ax),σ_{CO}) orbital has relatively large exterior electron distribution around the hydrogen atoms. The electron distribution of $5b_u$(σ_{CH}(eq),$\pi_{CO\perp}$) orbital extends outside around oxygen and equatorial hydrogen atoms. The very small negative slope of CEDPICS ($m = -0.023$) shows that the average contribution of repulsive interaction around the hydrogen atoms is large. The band 11 shows the more negative collision energy dependence in CERPIES than bands 9 and 10, probably due to the exterior electron distribution around the oxygen atoms of $5b_u$-(σ_{CH}(eq),$\pi_{CO\perp}$) orbital.

The band 12 is assigned to $5a_g$(σ_{CH}(eq),$\pi_{CO\parallel}$) orbital, although it has been assigned to b_u orbital in the semiempirical calculation.[45] Similar characteristics of this band is found in band 12 in tetrahydropyran. The strong band intensity in PIES, the large negative slope of m, and the negative peak energy shift for this band can be compared with band 12 in tetrahydropyran. The value of $|m|$ ($m = -0.293$) is larger than that of corresponding band in tetrahydropyran ($m = -0.218$) and tetrahydrofuran ($m = -0.220$). This is explained by the structure of containing two oxygen atoms. Because of relatively large component of oxygen the relative contribution of interaction around the hydrogen atoms is considered to be less effective.

The band 13 corresponds to the σ_{CH}(ax)(C_{2s}) orbital. As in the case of tetrahydropyran and tetrahydrofuran, this band can be related to the intramolecular Auger-like ionization process. The positive collision energy dependence reflecting the reaction around the carbon atoms was observed.

D. 1,3-Dioxane. Although UPS for 1,3-dioxane have been studied previously,[41,42] assignments of only a few bands have been discussed. Our assignments are listed in Table 4.

The bands 1 and 2 correspond to $n_{O\perp}$ and $n_{O\parallel}$ orbitals, which are close in energy. The large negative slope of CEDPICS ($m = -0.315$) and large negative peak energy shifts (-370 and -410 ± 150 meV) reflect the attractive interaction both in perpendicular and parallel direction of COC planes around the oxygen atoms.

The bands 3 and 4 correspond to 14a′(σ_{CO},σ_{CH}(eq)) and 8a″($n_{O\perp}$,σ_{CH}(ax)) orbitals. The 14a′ orbital has electron distribution in COC planes around the two oxygen atoms, and the 8a″ orbital extends out of the COC planes around the oxygen atoms. The large negative slope in the log σ vs log E_C plots ($m = -0.262$) is due to attractive interaction around the oxygen atoms. The smaller negative slope for the bands 3 and 4 in comparison with that for the bands 1 and 2 can be ascribed to the relative increase of exterior electron density around the hydrogen atoms well separated from oxygen atoms for 14a′ and 8a″ orbitals.

The band 5 is originated from 13a′(σ_{CH}(ax)) orbital. The electron distribution is predominantly around the axial hydrogen atom bonding to the carbon of the 5-position. The negative slope of CEDPICS is relatively large. This is probably because the axial hydrogen atom on the 5-position is in good proximity with lone-pair electrons of oxygen atoms in axial positions. This type of 1,3-diaxial interactions are crucially important for most stable conformation of substituted cyclohexanes such as methylcyclohexane, *cis*-1,3-dimethylcyclohexane, and *cis*-1,3-cyclohexanediol. The large negative peak energy shift due to the attractive interaction is observed in low collision energy spectrum in Figure 8. In high collision energy spectrum, the shoulder around 7.05 eV is stronger, which indicates the contribution of repulsive interaction around the axial hydrogen atom.

The bands 6 and 7 are assigned to 7a″ (σ_{CH}(eq),$\pi_{CO\parallel}$) and 12a′(σ_{CH}(eq)) orbitals, respectively. The value of slope parameter m of the log σ vs log E_C plots ($m = -0.258$) is very close to those for the bands 3, 4 and the band 12. This indicates that the relative importance of attractive interaction is as a whole similar for those bands. The negative peak energy shifts for bands 6 and 7 are smaller than those for the bands 3, 4 and the band 12. This is likely due to the more electron distribution around the 2-, 4- and 6-equatorial hydrogen atoms in 7a″ and 12a′ orbitals for the bands 6 and 7.

The bands 8 and 9 are originated from 6a″(σ_{CH}(ax,eq),$\pi_{CO\perp}$) and 11a′(σ_{CH}(eq),σ_{CO}) orbitals, respectively. The contribution of repulsive interaction around the hydrogen atoms is relatively large and the value of $|m|$ becomes smaller ($m = -0.165$). The band 8 is affected by attractive interaction more effectively than the band 9, in consistent with the larger peak energy shift. The PIES intensity of band 8 is relatively stronger than band 9. These are related to the exterior electron distribution around the oxygen atoms in 6a″(σ_{CH}(ax,eq),$\pi_{CO\perp}$) orbital. On the other hand, the 11a′(σ_{CH}(eq),σ_{CO}) orbital has an electron distribution around equatorial hydrogen atom on the 5-position far from the oxygen atoms.

The bands 10 and 11 correspond to σ_{CH}(ax) and σ_{CO} orbitals, respectively. Similar to the bands 8 and 9, the reaction around the hydrogen atoms is dominant and the value of $|m|$ is relatively small. As for the band intensity in PIES, the band 11 is weaker than the bands 8, 9 and 10. This is consistent with the assignment for the band 11 since the σ_{CO} orbital has little exterior electron distribution outside the molecular surface.

The large negative slope of CEDPICS ($m = -0.237$) and the strong band intensity for band 12 are related to a large electron distribution of 9a′(σ_{CH}(eq),$\pi_{CO\parallel}$) orbital around the oxygen atoms and equatorial hydrogen atoms along the in-plane direction in common phase, as in the case of other cyclic ethers mentioned above. Relatively smaller value of $|m|$ compared with the band 12 in 1,4-dioxane may be attributed to difference in the geometry of two oxygen atoms which leads to difference in effectiveness of the attractive well to affect the trajectory of He*.

The band 13 corresponds to σ_{CH}(ax)(C_{2s}) orbital. Positive slope of CEDPICS reflecting the selective reaction around the carbon atoms similarly to the case of other cyclic ethers.

E. Interaction around the Oxygen Atoms. As for the interaction potential around the oxygen atoms (Figures 13a, 14a, and 15a) for COC plane directions of which the $n_{O\parallel}$ orbital extends, the calculated potential curves show deep potential well of 450−500 meV with separations of about 2 Å in the directions bisecting COC angle. This is consistent with the experiment; the PIES bands corresponding to $n_{O\parallel}$ orbitals show large negative peak energy shifts and large negative slope in CEDPICS. The interaction potential around the oxy group with He* in in-plane directions is analogous to $(CH_3)_2O$ and these cyclic ethers, but the well depth of cyclic ethers is slightly deeper than $(CH_3)_2O$.

For the direction out of the COC plane (Figures 13b, 14b, and 15b), the calculated interaction potential curves for ±90° direction of which $n_{O\perp}$ orbital extends is repulsive, though the $n_{O\perp}$ bands in PIES show negative collision energy dependence and negative peak energy shifts. This is because the potential well region extends widely around oxygen atom to the outside directions of the COC plane.

In our previous study of $(CH_3)_2O$ and $(CH_3CH_2)_2O$,[26] the interaction around the oxygen atom in the COC plane direction is found to be more attractive than in out-of-plane direction. In the case of tetrahydropyran and tetrahydrofuran, the direct comparison for $n_{O\parallel}$ and $n_{O\perp}$ bands from CEDPICS is not possible because the $n_{O\parallel}$ bands and σ_{CH} bands are overlapping. As for the case of 1,4-dioxane, it is shown from the CEDPICS (Figure 11) that the $n_{O\parallel}$ band has larger negative slope (band 6, $m = -0.300$) than $n_{O\perp}$ band (band 3, $m = -0.277$). In the case of 1,3-dioxane, though the $n_{O\parallel}$ and $n_{O\perp}$ bands are slightly overlapping, the $n_{O\parallel}$ band (band 2) has larger collision energy dependence than $n_{O\perp}$ band (band 1) in CERPIES (Figure 8). In the view of peak energy shifts, the attractive interaction is to be stronger in in-plane direction. In general, the interaction potential around the oxygen atom is more attractive for in-plane direction similarly to the case of chain ethers.

In $(CH_3)_2O$ and $(CH_3CH_2)_2O$, the effects of attractive interaction around the oxygen atoms are considered to be weakened as the functional group becomes large, because the steric hindrance of ethyl group is serious in the case of $(CH_3CH_2)_2O$. In the present study, the steric hindrance of oxygen atom is found to be smaller in the case of cyclic ethers than $(CH_3CH_2)_2O$. This is because the vicinity of oxygen atom is not effectively surrounded by methylene groups due to the fixed conformation of cyclic ethers, though the size of the functional groups are comparable to the size those of $(CH_3CH_2)_2O$.

Although the calculated attractive potential well depths around the oxygen atoms are similar among cyclic ethers and $(CH_3)_2O$, the differences are seen for the extent of the potential well especially in the directions out of the COC plane. As can be clearly seen by comparing the Figure 13b with Figures 14b or 15b, the attractive well region around the oxygen atom in the out-of-plane direction is extending wider for tetrahydrofuran than tetrahydropyran, both in the C_2 and C_s conformer. This is obviously seen when the potential curves for ±60° are compared. This tendency found in the calculation is also obtained in the experiment. In the present experiment, very large negative slope was found for tetrahydrofuran (band 1, $m = -0.460$), while much smaller negative slope was observed for tetrahydropyran ($m = -0.258$). The difference between five-membered ring and six-membered ring is attributed to the difference in the conformations. As for tetrahydropyran, the axial hydrogens of β-carbon atoms are positioned geometrically close to the oxygen atoms compared with tetrahydrofuran.

The interaction potential curves for tetrahydrofuran are similar to those for $(CH_3)_2O$ in previous study,[26] both in the depth and shape of potential well. Thus, the resemblance of slope parameter between $n_{O\perp}$ bands of tetrahydrofuran ($m = -0.460$) and $(CH_3)_2O$ ($m = -0.379$) are considered to be reasonable.

VII. Conclusion

The oxygen lone pair bands of cyclic ethers in PIES show negative collision energy dependence of partial ionization cross sections in the collision energy range investigated. This is attributed to the attractive interaction potential around the oxygen atom, which is consistent with the calculated interaction potentials. The attractive interaction around the oxygen atoms is stronger for in-plane directions of COC than out-of-plane directions.

The effects of attractive interactions around the oxygen atom strongly depend on the stereochemical surroundings. The steric hindrance around oxygen atom in cyclic ethers is found to be much smaller than $(CH_3CH_2)_2O$ because of the fixed conformation of cyclic ethers compared with those of $(CH_3CH_2)_2O$.

Interesting aspects were found commonly in PIES for these cyclic ethers investigated. The PIES intensity of $\pi_{CO\parallel}$ bands is strong because the corresponding orbitals have large exterior electron density extending around oxygen and also around equatorial hydrogen atoms in common phase. The C_{2s} bands exhibit enhancement in PIES related to the intramolecular Auger-like ionization process as well as positive collision energy dependence reflecting the repulsive interaction around the carbon atoms. The relative PIES intensities for σ_{CO} orbitals which contribute to the ring skeletal structure are small because of small exterior electron densities. The large negative peak energy shifts in PIES were observed in $n_{O\parallel}$ bands.

Assignments of UPS of cyclic ethers, which have hardly been discussed previously, were performed on the basis of the collision energy dependence of partial ionization cross sections, collision energy resolved PIES, and ab initio MO calculations.

Acknowledgment. We thank Kohji Okamura for his help in experiment and discussion. This work has been supported by a Grant-in-Aid for Scientific Research from Japanese Ministry of Education, Science, and Culture.

References and Notes

(1) Penning, F. M. *Naturwissenschaften* **1927**, *15*, 818.
(2) Niehaus, A. J. *Adv. Chem. Phys.* **1981**, *45*, 399.
(3) Yencha, A. J. *Electron spectroscopy; Theory, Technique, and Applications*; Bundle, C. R., Baker, A. D., Eds.; Academic: New York, 1984; Vol. 5.
(4) Illenberger, E.; Neihaus, A. *Z. Phys. B* **1975**, *20*, 33.
(5) Parr, T. P.; Parr, D. M.; Martin, R. M. *J. Chem. Phys.* **1982**, *76*, 316.
(6) Pesnelle, A.; Watel, G.; Mamus, C. *J. Chem. Phys.* **1975**, *62*, 3590.
(7) Woodard, M. R.; Sharp, R. C.; Seely, M.; Muschlitz, E. E., Jr. *J. Chem. Phys.* **1978**, *69*, 2978.
(8) Appolloni, L.; Brunetti, B.; Hermanussen, J.; Vecchiocattivi, F.; Volpi, G. G. *J. Chem. Phys.* 1987, *87*, 3804.
(9) Allison, W.; Muschlitz, E. E., Jr. *J. Electron Spectrosc. Relat. Phenom.* **1981**, *23*, 339.
(10) Riola, J. P.; Howard, J. S.; Rundel, R. D.; Stebbings, R. F. *J. Phys. B* **1974**, *7*, 376.
(11) Lindinger, W.; Schmeltekopf, A. L.; Fehsenfeld, F. C. *J. Chem. Phys.* **1974**, *61*, 2890.
(12) Čermák, V. *J. Chem. Phys.* **1966**, *44*, 3781.
(13) Hotop, H.; Niehaus, A. *Z. Phys. B* **1969**, *228*, 68.
(14) (a) Ohno, K.; Mutoh, H.; Harada, Y. *J. Am. Chem. Soc.* **1983**, *105*, 4555. (b) Ohno, K.; Harada, Y. In *Theoretical Models of Chemical Bonding*; Maksič, Z. B., Ed.; Springer-Verlag: Berlin, 1991; Part 3, pp 199−234.
(15) Mitsuke, K.; Takami, T.; Ohno, K. *J. Chem. Phys.* **1989**, *91*, 1618.
(16) Ohno, K.; Takami, T.; Mitsuke, K.; Ishida, T. *J. Chem. Phys.* **1991**, *94*, 2675.
(17) Takami, T.; Mitsuke, K.; Ohno, K. *J. Chem. Phys.* **1991**, *95*, 918.
(18) Takami, T.; Ohno, K. *J. Chem. Phys.* **1992**, *96*, 6523.
(19) Dunlavy, D. C.; Martin, D. W.; Siska, P. E. *J. Chem. Phys.* **1990**, *93*, 5347.
(20) Longley, E. J.; Dunlavy, D. C.; Falcetta, M. F.; Bevsek, H. M.; Siska, P. E. *J. Phys. Chem.* **1993**, *97*, 2097.
(21) Siska, P. E. *Rev. Mod. Phys.* **1993**, *65*, 337.
(22) Pasinszki, T.; Yamakado, H.; Ohno, K. *J. Phys. Chem.* **1993**, *97*, 12718.
(23) Ohno, K.; Kishimoto, N.; Yamakado, H. *J. Phys. Chem.* **1995**, *99*, 9687.
(24) Ohno, K.; Okamura, K.; Yamakado, H.; Hoshino, S.; Takami, T.; Yamauchi, M. *J. Phys. Chem.* **1995**, *99*, 14247.
(25) Pasinszki, T.; Yamakado, H.; Ohno, K. *J. Phys. Chem.* **1995**, *99*, 14678.
(26) Yamakado, H.; Yamauchi, M.; Hoshino, S.; Ohno, K. *J. Phys. Chem.* **1995**, *99*, 17093.
(27) Kishimoto, N.; Yamakado, H.; Ohno, K. *J. Phys. Chem.* **1996**, *100*, 8204.
(28) Mitsuke, K.; Kusafuka, K.; Ohno, K. *J. Phys. Chem.* **1989**, *93*, 3062.
(29) Gardner, J. L.; Samson, J. A. R. *J. Electron Spectrosc. Relat. Phenom.* **1976**, *8*, 469.
(30) Kimura, K.; Katsumata, S.; Achiba, Y.; Yamazaki, T.; Iwata, S. *Handbook of He I Photoelectron Spectra of Fundamental Organic Molecules*; Japan Scientific: Tokyo, 1981.
(31) Frisch, M. J.; Trucks, G. W.; Head-Gordon, M.; Gill, P. M.; Wong, M. W.; Foresman, J. B.; Johnson, B. G.; Schlegel, H. B.; Robb, M. A.; Replogel, E. S.; Gomperts, R.; Andres, J. L.; Raghavachari, K.; Binkley, J. S.; Gonzalez, C.; Martin, R. L.; Fox, D. J.; Defrees, D. J.; Baker, J.; Stewart, J. J. P.; Pople, J. A. *Gaussian 92*; Gaussian, Inc.: Pittsburgh, PA, 1992.
(32) Breed, H. E.; Gundersen, C.; Seip, R. *Acta Chem. Scand.* **1979**, *A33*, 225.
(33) Almennigen, A.; Seip, H. M.; Willadsen, T. *Acta Chem. Scand.* **1969**, *23*, 2748.
(34) Davis, M.; Hassei, O. *Acta Chem. Scand.* **1971**, *25*, 725.
(35) Allinger, N. L.; Chung, D. Y. *J. Am. Chem. Soc.* **1976**, *98*, 6978.
(36) Rothe, E. W.; Neynaber, R. H.; Trujillo, S. M. *J. Chem. Phys.* **1965**, *42*, 3310.
(37) Hotop, H. *Radiat. Res.* **1974**, *59*, 379.
(38) Haberland, H.; Lee, Y. T.; Siska, P. E. *Adv. Chem. Phys.* **1981**, *45*, 487.
(39) Handy, N. C.; Marron, M. T.; Silverstone, H. J. *Phys. Rev.* **1969**, *180*, 45.
(40) Morrell, M. M.; Parr, R. G.; Levy, M. *J. Chem. Phys.* **1975**, *62*, 549.
(41) Kobayashi, T.; Nagakura, S. *Bull. Chem. Soc. Jpn.* **1979**, *46*, 1558.
(42) Sweigart, D. A.; Turner, D. W. *J. Am. Chem. Soc.* **1972**, *94*, 5599.
(43) Schmidt, H.; Schweig, A. *Chem. Ber.* **1974**, *107*, 725.
(44) Gerson, S.; Worley, S.; Bodor, N.; Kaminski, J.; Flechtner, T. *J. Electron Spectrosc. Relat. Phenom.* **1978**, *13*, 421.
(45) Bieri, G.; Åsbrink, L.; von Niessen, W. *J. Electron Spectrosc. Relat. Phenom.* **1982**, *27*, 129.
(46) Yee, D. S. C.; Hamnett, A.; Brion, C. E. *J. Electron Spectrosc. Relat. Phenom.* **1976**, *8*, 291.
(47) Niehaus, A. *Ber. Bunsen-Ges. Phys. Chem.* **1973**, *77*, 632.
(48) Takami, T.; Mitsuke, K.; Ohno, K. *J. Chem. Phys.* **1991**, *92*, 2.
(49) Seip, H. M. *Acta Chem. Scand.* **1969**, *23*, 2741.
(50) Cremer, D.; Pople, J. A. *J. Am. Chem. Soc.* **1975**, *97*, 1358.
(51) Cadioli, B.; Gallinella, E.; Coulombeau, C.; Jobic, H.; Berthier, G. *J. Phys. Chem.* **1993**, *97*, 7844.
(52) Dobado, J. A.; Molina, J. M.; Espinosa, M. R. *J. Mol. Struct. (THEOCHEM)* **1994**, *303*, 205.
(53) Engerholm, G. G.; Luntz, A. C.; Gwinn, W. D.; Harris, D. O. *J. Chem. Phys.* **1969**, *50*, 2446.
(54) Geise, H. J.; Adams, W. J.; Cartell, L. S. *Tetrahedron* **1969**, *25*, 3045.